High-Gain and Wide-Bandwidth Filtering Planar Antenna Array-Based Solely on Resonators

Rashad H. Mahmud and Michael J. Lancaster, *Senior Member, IEEE*

***Abstract*— This paper presents a new approach for the design of high-gain and wide-bandwidth planar antenna arrays. It is based on the coupling matrix theory which allows the design of the arrays using all-resonator structures. The parameters of the matrix offer the flexibility of achieving a controllable bandwidth. They also introduce a frequency filtering functionality into the arrays which can remove the need to place a bandpass filter after the arrays at the very front end of a communication system. The new approach has been applied to using novel topologies to form two wideband 4 × 4 planar antenna arrays utilizing rectangular waveguide cavity resonators operated at X-band frequencies. The first topology is seventh order and based on 39 resonators configured in two waveguide-layers; that is one layer for the feed resonators and one layer for the radiating resonators. The second topology is fourth order based on 25 resonators configured only in a single waveguide-layer. Fabrication and measurements have been performed, showing very good agreement with the simulations.**

***Index Terms*— Bandpass filter (BPF), coupling matrix theory, filtering planar antenna arrays, high-gain and wide-bandwidth planar antenna array.**

I. Introduction

HIGH gain, wide bandwidth, and small size are the properties of antennas, which are required in many modern wireless communication systems [1]. There has been an increasing interest in using slotted waveguide antenna arrays in many high-gain antenna applications due to ease in achieving high gains by making more slots in the walls of the waveguides. Also, because they are mostly air-filled, they do not suffer from dielectric losses. Conventionally, a series-fed network is employed in a single waveguide-layer to design a planar array slotted waveguide antenna [2]–[8]. Such feeding networks offer unique features for the array such as using only a single waveguide-layer structure to form the whole antenna array, and hence simplifying the fabrication process. However, its main disadvantage is the reduction of the bandwidth of the arrays due to the "long-line" effect [1], [9], [10]. Therefore, to overcome the bandwidth issue, a halved feeding technique is introduced to the single waveguide-layer antenna array in [11] to reduce the long-line effect by a factor of two due to the feeding of the array at the center. Also, the quartered feeding network, which divides the array into four subarrays and still utilizes a single waveguide-layer, is demonstrated in [12]. This is to reduce the long-line effect by a factor of four. Later, the idea of double waveguide-layers is proposed in [13] and [14] to design wide bandwidth and high efficient slotted waveguide antenna arrays. The lower layer is allocated to build the feeding network, and the top layer is to form the array. Based on this idea, there have been interesting designs of wide bandwidth slotted waveguide antenna arrays, notably 4 × 4 [15], 8 × 8 [1], and 16 × 16 [10], [16] arrays. In this paper, we utilize the coupling matrix as a new approach to design wide bandwidth planar array waveguide aperture antennas for the first time. This approach, as well adding the frequency filtering functionality feature, can remove the need of the additional waveguide-layer to design wide bandwidth large aperture antenna arrays.

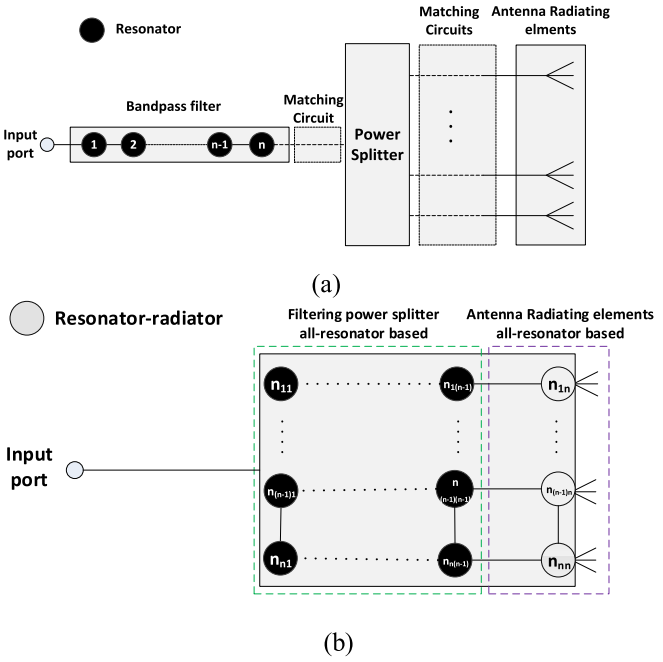

Fig. 1. Schematic of (a) conventional cascaded BPF, power splitter, and an antenna array at the RF front end of a communication system, and (b) proposed filtering planar antenna array based on n-coupled resonators.

Traditionally, the coupling matrix is an approach used to design a two-port bandpass filter (BPF) circuit, which is usually built from n-coupled-resonators, placed after a receiving and/or a transmitting antenna at the very front end of a communication system [see Fig. 1(a)]. This filter is to

Manuscript received April 30, 2016; revised December 15, 2016; accepted December 21, 2016. Date of publication March 17, 2017; date of current version May 3, 2017. This work was supported by the U.K. Engineering and Physical Science Research Council under Contract EP/H029656/1.

R. H. Mahmud was with the School of Electronics, Electrical and Systems Engineering, University of Birmingham, Birmingham B15 2TT, U.K. He is now with the Physics Department, Salahaddin University-Erbil, Kurdistan Region, Iraq (e-mail: rhm11286@yahoo.co.uk).

M. J. Lancaster is with the School of Electronics, Electrical and Systems Engineering, University of Birmingham, Birmingham B15 2TT, U.K.

Color versions of one or more of the figures in this paper are available online at http://ieeexplore.ieee.org.

Digital Object Identifier 10.1109/TAP.2017.2670443

pass the signals within the frequency band of interest and attenuate them at out of the bands [17]–[19]. The design concept of multiple-port circuits, all resonator-based, was first introduced in [20]; here the basic two-port filter was extended to multiple ports enabling all resonator-based power splitters, diplexers and multiplexers to be constructed [21]–[23]. The idea of the filtering power splitter using the coupling matrix theory is detailed in [21] and is of interest here due to the fact that the filtering power splitters can provide a controllable bandwidth to the antenna array, particularly if the antenna elements are considered as resonators. In this paper, we develop the coupling matrix approach one step further to design a component which combines the features of a BPF, power splitters, and an antenna array [see Fig. 1(b)]. We apply this theory to generate a wideband planar antenna array. We call this component *filtering planar antenna array*. In this way, in addition to providing a controllable bandwidth for the antenna array, a significant reduction in the size of the communication system can be achieved due to the reduction of the number of components by removing the need for matching circuits and using the antenna elements as resonators in the bandpass networks [see Fig. 1(a) compared with Fig. 1(b)].

The integration of antennas with BPFs has been investigated extensively in the last few decades, and the filter synthesis principles are widely utilized in most of the investigations as a design tool. In addition, the integration is mostly applied to small array structures (maximum 2×2 arrays). A simple single waveguide slot antenna which is resonator-based has been integrated with four coupled-resonators using the two-port filter synthesis in [24]. In [25], a filter with an 2×2 antenna array is integrated vertically to reduce the footprint. A filtering monopulse antenna array is proposed in [26]. The array has four radiating elements, and the four output filter including the monopulse comparator is designed by modifying the coupling matrix of a single-ended filter technique. He we present arrays with much large number of elements and consequently improved filtering characteristics and in conventional waveguide. We also detail the coupling matrix approach. A new 2×2 microstrip filtering antenna array including a very compact feeding network is presented in [27]. Later, in [28], a slotted waveguide antenna array is demonstrated when integrating with a T-shaped filter. In this paper, in addition to developing the multiport coupling matrix approach to integrate antenna arrays with PBFs, we have implemented the approach for the first time on the two novel relatively large array topologies (4×4 arrays).

This paper is organized as follows. Details regarding the coupling matrix are given in Section II. This is followed by the extraction technique of the parameters of the coupling matrix using TE_{101} mode rectangular waveguide cavity resonators. The topologies of the two novel filtering planar antenna arrays, a seventh-order 4×4 *filtering planar antenna array* and a fourth-order 4×4 *filtering planar antenna array*, are discussed in Sections III and IV. Their fabrication, measurements, and comparison with the theoretical expectations are presented and discussed in Section V. This is followed by conclusions obtained in this paper in Section VI.

II. Coupling Matrix Approach

The design of a two-port filter circuit using just resonators based on the coupling matrix theory is discussed in [19], and is extended in [21] to design filtering multiple-ports circuits such as diplexers, multiplexers and power splitters. In this paper, the coupling matrix for the *filtering planar antenna array* [Fig. 1(b)] is derived in a similar way to the filtering power splitter circuit discussed in [21], except here the output of the *filtering planar antenna array* is considered to launch to free space, instead of being coupled to electric ports.

The advantage of using the coupling matrix is to allow formal design of the filtering antenna array by a fast analytical approach. The exact requirement of the filtering part of the antenna array can be specified and the coupling between resonators, or to the external world, can then calculated. Using this information the resonators (including the antenna resonant radiating elements) can be dealt with one or two at a time building up the antenna structure. This allows a large structure with many resonators to be designed. The final part of the design is a final full-wave optimization, but this is quick as the coupling matrix method has determined a very close to final structure.

The general normalized matrix $[A]$ can be expressed in terms of the scaled coupling coefficients and external/radiation quality factors as follows [19]:

$$[A] = \begin{bmatrix} \frac{1}{q_{e1}} & \cdots & 0 & 0 \\ \vdots & \ddots & \vdots & \vdots \\ 0 & \cdots & \frac{1}{q_{r(n-1)}} & \vdots \\ 0 & \cdots & \vdots & \frac{1}{q_{rn}} \end{bmatrix} + p \begin{bmatrix} 1 & \cdots & 0 & 0 \\ \vdots & 1 & \vdots & 0 \\ 0 & \cdots & \ddots & \vdots \\ 0 & \cdots & 0 & 1 \end{bmatrix} - j \begin{bmatrix} m_{11} & \cdots & m_{1(n-1)} & m_{1n} \\ \vdots & \ddots & \vdots & \vdots \\ m_{(n-1)1} & \cdots & m_{(n-1)(n-1)} & m_{(n-1)n} \\ m_{n1} & \cdots & m_{n(n-1)} & m_{nn} \end{bmatrix}$$

where q_{ei} ($q_{ei} = Q_{ei}\text{FBW}$) is the scaled external quality factor of the resonator i coupled to the port. Q_{ei} is the nonscaled external quality factor used for its extraction from the physical structure (waveguide iris in the design here and described in the following) attached to the resonator i. FBW is the fractional bandwidth chosen for the *filtering planar antenna array*. q_{rn} ($q_{rn} = Q_{rn}\text{FBW}$) is the scaled radiation quality factor of the resonator-radiators one for each of the radiating elements of the *filtering planar antenna array* [see Fig. 1(b)]. These are coupled into free space. Q_{rn} is the nonscaled radiation quality factor used for the design of the radiating apertures in each of the resonator-radiators. p ($p = j/\text{FBW}(\omega/\omega_0 - \omega_0/\omega)$ is the complex frequency variable, ω_0 and ω are the angular centre frequency and the angular frequency. m_{ij} ($m_{ij} = M_{ij}/\text{FBW}$) is the scaled coupling coefficient between resonators i and j. M_{ij} is the nonscaled coupling coefficient used for its extraction from the physical structure (iris) placed between resonators i and j. m_{ii} is the self-coupling coefficient for resonator i when it is asynchronously tuned. The mutual coupling effect

between the radiating outputs (resonator-radiators) can be accounted for this approach by terms in the coupling matrix. However, it has not been considered in the presented designs. It should be noted that the mutual coupling is found to be small as the coupling matrix calculated corresponds well to the final solution in the filtering antenna arrays described here. That is none of the coupling terms in the matrix representing coupling between the antenna elements are required to determine the antenna properties from the coupling matrix. The reflection scattering parameter of the *filtering planar antenna array* (which is derived in [19] for filters), may be expressed in terms of the general normalized matrix $[A]$ as follows:

$$S_{11} = 1 - \frac{2}{q_{ei}} \cdot [A]^{-1}_{11} \tag{1}$$

where S_{11} is the reflection coefficient [19]. Here we take the input external Q_{ei} values to be equal to the resonator-radiator Q_{rn} values. In the design method described in the following, the extraction technique of Q_{ei} is different than Q_{rn} due to the fact that the resonator-radiators launch into free space, instead of coupling into electrical ports. For a particular filter-antenna specification, it is straightforward to calculate the values of Q_{ei}, Q_{rn} and M_{ij} using the techniques described in [19]. The response can then be calculated using (1). However, these values then need to be related to the physical dimensions of the waveguide structure forming the *filtering planar antenna array*. This is described in Sections II-A, II-B, and II-C, with the extraction of the parameters Q_{ei}, Q_{rn}, and M_{ij} explained in detail and accomplished with the aid of full-wave simulations (CST microwave studio) [29]. It should be mentioned that although the approximations in the coupling matrix are inherently narrow band all resonator-based filters [30], multiplexers [23], and hence filtering antennas can be produced in wider bandwidths if the couplings are available in the particular fabrication technology (such as waveguide). Generally deviations from the narrowband approximation can be corrected for in full-wave optimization.

A. External Quality Factor (Q_{ei})

This section discusses a technique used for the extraction of Q_{ei} of the waveguide resonators forming the input to the *filtering planar antenna array* [19]. The structure used is shown in the inset of Fig. 2 and modeled in CST [29]. It consists of a single lossless rectangular waveguide cavity resonator which is coupled to input and output ports via irises. Although capacitive or inductive irises can be used to couple the resonator to the ports in principle, only capacitive iris is chosen here due to it providing a wide variation of Q_{ei} values versus the iris width (d_0). The S_{21} parameter, obtained from the structure using CST, is used for the calculation of Q_{ei} using the relationship between the resonant frequency f_0 of the cavity and 3-dB bandwidth $\Delta f_{3\,\mathrm{dB}}$ as follows:

$$Q_{ei} = \frac{f_0}{\Delta f_{(3\mathrm{dB})}}. \tag{2}$$

f_0, Δf, and Q_{ei} values vary when the cavity length l and the iris width d_0 are altered. These variations are plotted in Fig. 2. It can be seen that Q_{ei} reduces when d_0 increases. To obtain the required Q_{ei} value, the l_1 dimension needs to be tuned in order to keep the f_0 at the desired center frequency, in this paper 10 GHz. The thicknesses (t) of the irises are kept at 2 mm in order to simplify the extraction process. Also, the h_o dimension is chosen to be very small (0.04 mm) providing weak coupling in order to extract Q_{ei} versus d_0 precisely. The Q_{ei} curve plotted in Fig. 2 will be used to obtain the d_0 of the *filtering planar antenna array* presented in Section III. The technique presented here can also be used to obtain the d_0 dimension of the array in Section IV, except that the capacitive irises are to be changed to inductive irises.

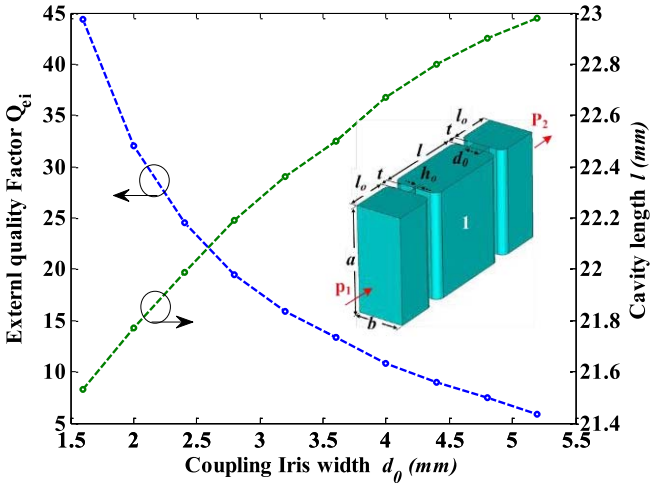

Fig. 2. Structure modeled in CST for the extraction of Q_{ei} is shown in the inset. Dimensions in mm, $a = 22.86$, $b = 10.16$, $l_0 = 10.16$, $h_0 = 0.04$, and $t = 2$.

B. Coupling Coefficient (M_{ij})

This section explains the extraction of M_{ij} between two coupled-resonators which are utilized in the construction of the *filtering planar antenna arrays*. The structure used is shown in the inset of Fig. 3 and is modeled with CST. The structure is two lossless waveguide resonators coupled together via irises. The resulting S_{21} shows two peak values at the frequencies (f_1, f_2) [31]. The value of the M_{ij} can be determined in accordance with these two frequency values using the following:

$$M_{ij} = \frac{f_1^2 - f_2^2}{f_1^2 + f_2^2}. \tag{3}$$

The orientation of the coupled-resonators determines the nature of the coupling (electric or magnetic). Here, we have decided to use capacitive irises (electric coupling) to make the coupling between the coupled-resonators of the *filtering planar antenna arrays* as strong as possible in order to realize the required wide bandwidth of the circuit [32], [33]. The two rectangular waveguide cavity resonators, shown in the inset of Fig. 3, are coupled to each other with aperture widthd_k. The variation of M_{ij} versus d_k is obtained using (3), and is also shown in Fig. 3. One can see that M_{ij} value increases with an increase of d_k. The length of the resonators l_1 is adjusted here

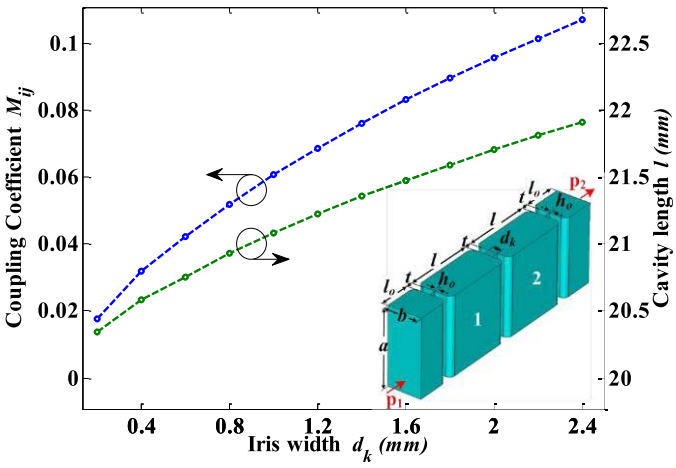

Fig. 3. Structure modeled in CST for the extraction of M_{ij} between two electrically coupled-resonators is shown in the inset. Dimensions in mm, $a = 22.86$, $b = 10.16$, $l_0 = 10.16$, $h_0 = 0.04$, and $t = 2$.

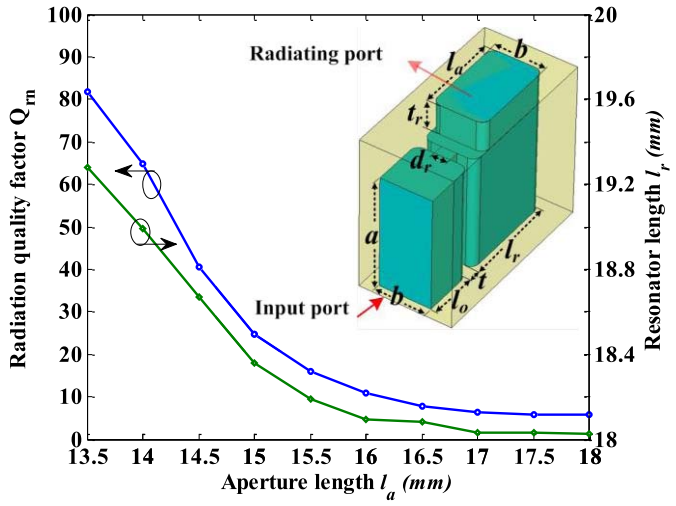

Fig. 4. Structure modeled in CST for the extraction of Q_{rn} is shown in the inset. Dimensions in mm, $a = 22.86$, $b = 10.16$, $d_r = 1$, $l_0 = 10.16$, $t_r = 10$, and $t = 2$.

in order to keep the center frequency at 10 GHz, and to do this it is seen that an increase in the l_1 value is required. The curve shown in Fig. 3 is utilized to obtain the d_k dimensions of the electrically coupled-resonators in Sections III and IV. The same technique can be applied to obtain the d_k dimension between those resonators which are coupled via inductive irises (magnetic coupling).

C. Radiation Quality Factor (Q_{rn})

This section discusses the extraction of the Q_{rn} of a single cavity resonator-radiator when it is coupled into by a single external port, utilizing the magnitude of S_{11} from a CST simulation. We have already discussed that the calculation of Q_{ei} for a two-port cavity resonator can be undertaken by using the magnitude of S_{21} in Section II-A. However, for the case of the resonator-radiator, the S_{21} parameter is not easily available. An alternative technique is therefore necessary.

A lossless waveguide cavity resonator-radiator, which is shown in the inset of Fig. 4, and designed here using CST, has a loaded quality factor Q_l, which can be calculated by [19]

$$\frac{1}{Q_l} = \frac{1}{Q_{ei}} + \frac{1}{Q_{rn}} \tag{4}$$

where, Q_{ei} is the external quality factor, and Q_{rn} is the radiation quality factor obtained only from the radiating port. The Q_{rn} value, based on the magnitude of S_{11} of the cavity, can be computed by [34], [35]

$$Q_{rn} = \frac{1}{|\Delta f_a|}\left[\frac{|S_{11}(f_a)|^2(1+\beta)^2 - (1-\beta)^2}{1-|S_{11}(f_a)|^2}\right]^{1/2} \tag{5}$$

where $\Delta f_a = 1 - (f_0^2/f_a^2)$. f_0 is the resonant frequency, and f_a is a frequency point other than the resonant frequency in the passband range. In order to increase the accuracy of the Q_{rn} value corresponding to a single cavity resonator-radiator dimension (l_a), we use around 50 different points of $f_a$and average the values**.** The coupling coefficient β between the external circuit and the resonator-radiator can be given by [34]

$$\beta = \frac{P_r}{P_0} = \frac{Q_{rn}}{Q_{ei}} \tag{6}$$

where P_o is average power loss to external circuit and P_r is average power loss to radiation.

In the structure shown in the inset of Fig. 4, a capacitive iris is used to couple the resonator-radiator to the input port. The boundary in CST is defined to be open in all directions. For the calculation of the Q_{rn}, it is assumed that the resonator-radiator is weakly coupled to the port. This leads us to an approximation of the value of Q_{ei} approaches to infinity. This means the β value vanishes ($\beta \cong 0$). After applying this approximation into (4), we can now assume that $Q_l = Q_{rn}$. The parameters β and f_a in (5) can be calculated precisely which is explained in detail in [34].

The physical dimensions l_a and l_r of the resonator-radiator, which are labeled in the inset of the structure shown in Fig. 4, are utilized to obtain the target Q_{rn} at the resonant frequency f_0. It should be mentioned that the l_a value is chosen for the *filtering planar antenna array* that provides a Q_{rn} value which is equal to the Q_{ei}. In this way, the array obtains a frequency response which is comparable to the response obtained from the coupling matrix. This will be seen in Sections III and IV. The variation of Q_{rn} versus l_a is plotted in Fig. 4, and it can be seen that the Q_{rn} value dramatically increases when l_a is reduced. The value of l_r is tuned to keep f_0 at center frequency of 10 GHz. The technique discussed here will be utilized to obtain the radiating aperture dimensions of the resonator-radiators of the *filtering planar antenna arrays* given in Sections III and IV.

III. Topology-I

Fig. 5 shows the resonator layout for the seventh-order 4×4 *filtering planar antenna array*. It consists of 39 resonators. There are seven resonators that contribute to each radiating path, and four resonator**s** in the topology to split the input power into sixteen outputs equally. Each resonator in the

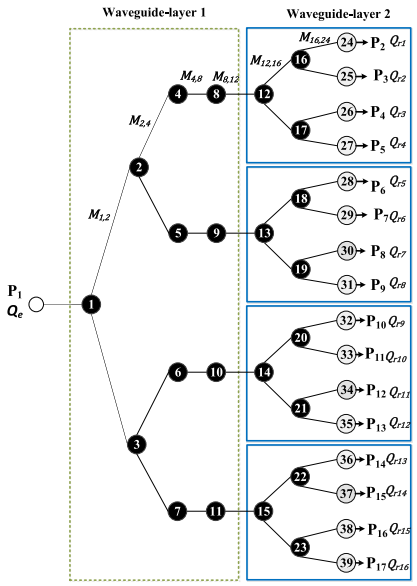

Fig. 5. Topology I for the seventh-order 4 × 4 filtering planar antenna array.

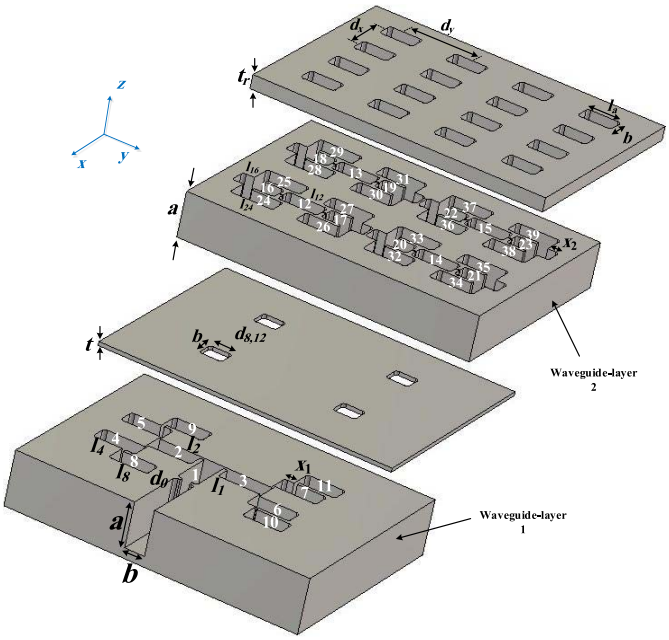

Fig. 6. Layout view of the topology-I modeled in the CST. The physical dimensions in mm are: $a = 22.86$, $b = 10.16$, $t = 2$, $t_r = 10$, $l_a = 17.272$, $d_x = 24.32$, $d_y = 34.31$, $x_1 = 5.120$, and $x_2 = 6.017$. The resonator lengths are: $l_1 = 25.323$, $l_2 = l_3 = 22.445$, $l_4 = l_5 = l_6 = l_7 = 21.784$, $l_8 = l_9 = l_{10} = l_{11} = 19.793$, $l_{12} = l_{13} = l_{14} = l_{15} = 20.437$, $l_{16} = l_{17} = l_{18} = l_{19} = l_{20} = l_{21} = l_{22} = l_{23} = 21.581$, and $l_{24} = l_{25} = l_{26} = l_{27} = l_{28} = l_{29} = l_{30} = l_{31} = l_{32} = l_{33} = l_{34} = l_{35} = l_{36} = l_{37} = l_{38} = l_{39} = 20.041$. The iris widths are: $d_0 = 4.978$, $d_{1,2} = d_{1,3} = 1.715$, $d_{2,4} = d_{2,5} = d_{3,6} = d_{3,7} = 0.913$, $d_{4,8} = d_{5,9} = d_{6,10} = d_{7,11} = 1.686$, $d_{8,12} = d_{9,13} = d_{10,14} = d_{11,15} = 11.571$, $d_{12,16} = d_{12,17} = d_{13,18} = d_{13,19} = d_{14,20} = d_{14,21} = d_{15,22} = d_{15,23} = 0.69$, and $d_{16,24} = d_{16,25} = d_{17,26} = d_{17,27} = d_{18,28} = d_{18,29} = d_{19,30} = d_{19,31} = d_{20,32} = d_{20,33} = d_{21,34} = d_{21,35} = d_{22,36} = d_{22,37} = d_{23,38} = d_{23,39} = 5.773$. Radius of the round corners = 1.6.

topology is coupled into no more than three resonators in order to simplify the physical implementation. The electrical specification is chosen to have 10% FBW and a return loss S_{11} of −20 dB over the passband (9.5–10.5 GHz).

The coupling matrix for the component has been obtained by using the gradient-based optimization technique [21]. The optimized normalized non-zero entries of the coupling matrix are: $m_{1,2} = m_{1,3} = 0.588$, $m_{2,4} = m_{2,5} = m_{3,6} = m_{3,7} = 0.424$, $m_{4,8} = m_{5,9} = m_{6,10} = m_{7,11} = 0.564$, $m_{8,12} = m_{9,13} = m_{10,14} = m_{11,15} = 0.564$, $m_{12,16} = m_{12,17} = m_{13,18} = m_{13,19} = m_{14,20} = m_{14,21} = m_{15,22} = m_{15,23} = 0.420$, $m_{16,24} = m_{16,25} = m_{17,26} = m_{17,27} = m_{18,28} = m_{18,29} = m_{19,30} = m_{19,31} = m_{20,32} = m_{20,33} = m_{21,34} = m_{21,35} = m_{22,36} = m_{22,37} = m_{23,38} = m_{23,39} = 0.588$. The scaled external and radiation quality factors are $q_e = q_{r1} = q_{r2} = \cdots = q_{r15} = q_{r16} = 1.0080$.

The topology has been incorporated into a physical structure using two waveguide-layers shown in Fig. 6. All the resonators are coupled with capacitive irises between them, except between resonators 8–12, 9–13, 10–14, and 11–15 where inductive irises are utilized in order to maintain vertical coupling between the layers and form the planar array configuration. The dimensions of the seventh-order 4 × 4 *filtering planar antenna array* are given in the caption of Fig. 6. Careful consideration has been made to maintain the phase across the resonator-radiator outputs and to provide the highest directivity possible.

The simulated frequency response of the seventh-order 4 × 4 *filtering planar antenna array* is obtained using the CST simulator [29] and compared in Fig. 7, with the ideal response obtained from the coupling matrix. It should be noted that the values of dimensions of the structure obtained via the techniques as described in Sections II-A–II-C provide good initial values to an optimization process in CST. However, the time required to obtain the response in Fig. 7 is still long due to the large electrical size of the array. To remedy this,

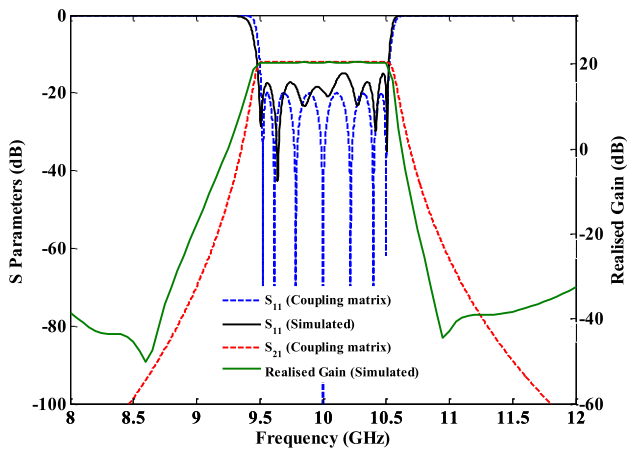

Fig. 7. Simulated frequency responses compared with the calculated of the order 4 × 4 *filtering planar antenna array*.

the symmetry plane feature in CST, which is a feature that allows simulating only half of the array [electric symmetry plane ($E_t = 0$) along the xz plane], is utilized. This is considered to reduce the computation time by the factor of two. The obtained simulated return loss (S_{11}) is below −15 dB over the passband. The realized gain is extremely flat over the passband, and has strong attenuation outside of the passband.

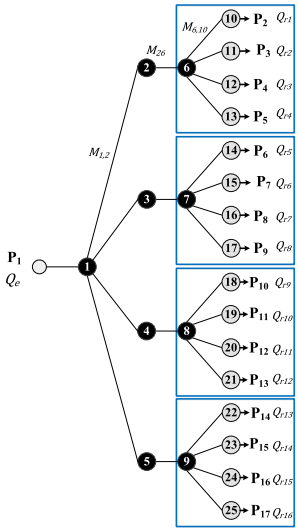

Fig. 8. Topology II for the fourth-order 4×4 filtering planar antenna array.

The simulated directivity is 20.57 dBi at the center frequency 10 GHz. There are two transmission zeros which appear near the passband edges. The nature of the couplings between resonators 4–8 and 16–24, which create a double path for the signal inside the resonators 4 and 16, are responsible for the creation of such kinds transmission zeros [36], [37]. Such a kind of coupling is configured in all the radiating paths of the array, but is not a general problem.

IV. Topology-II

Fig. 8 shows the resonator layout of the fourth-order 4×4 *filtering planar antenna array*. It consists of 25 resonators. Junctions with up to five couplings are implemented in the topology in order to offer size reduction. The input port is at the left-hand side of Fig. 8, and the output consists of sixteen resonators contributing to build the 4×4 array. Five identical four-way resonator power splitters are utilized in the topology so as to split the input signal into sixteen outputs. The gradient-based optimization technique [21] is used to generate an equivalent coupling matrix for the topology. The non-zero entries of the coupling matrix, and scaled external and radiation quality factors are: $m_{1,2} = m_{1,3} = m_{1,4} = m_{1,5} = 0.456$, $m_{2,6} = m_{3,7} = m_{4,8} = m_{5,9} = 0.700$, $m_{6,10} = m_{6,11} = m_{6,12} = m_{6,13} = m_{7,14} = m_{7,15} = m_{7,16} = m_{7,17} = m_{8,18} = m_{8,19} = m_{8,20} = m_{8,21} = m_{9,22} = m_{9,23} = m_{9,24} = m_{9,25} = 0.456$, $q_e = q_{r1} = q_{r2} = \cdots = q_{r15} = q_{r16} = 0.931$.

The topology used for the actual physical structure is shown in Fig. 9. It is proposed to construct this using only a single waveguide-layer containing all the resonators. The structure is symmetric in both of the E- and H-planes. This again allows the use of the symmetry plane feature to reduce the computational time required by CST [29]. The optimized simulated frequency response is plotted in Fig. 10. There is a very good agreement obtained between the simulation and the desired response obtained from the coupling matrix. The simulated directivity is 20.46 dBi at the center frequency 10 GHz. The narrow-wall widths (b_1) of the resonators $2, 3, \ldots, 9$ are chosen to be 7 mm in order to reduce the component size

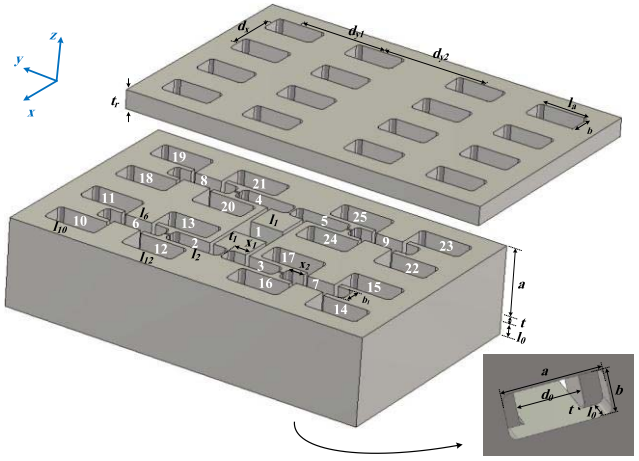

Fig. 9. Layout view of the topology II modeled in the CST. The physical dimensions in mm are: $a = 22.86$, $b = 10.16$, $b_1 = 7$, $t = 2$, $t_r = 10$, $l_0 = 8$, $l_a = 17$, $d_x = 21.16$, $d_{y1} = 32.22$, $d_{y2} = 41.98$, $x_1 = 5.22$, and $x_2 = 6.21$. The resonator lengths are: $l_1 = 15.70$, $l_2 = l_3 = l_4 = l_5 = 21.20$, $l_6 = l_7 = l_8 = l_9 = 25.62$, and $l_{10} = l_{11} = l_{12} = l_{13} = l_{14} = l_{15} = l_{16} = l_{17} = l_{18} = l_{19} = l_{20} = l_{21} = l_{22} = l_{23} = l_{24} = l_{25} = 20.38$. The iris widths are: $d_0 = 15.68$, $d_{1,2} = d_{1,3} = d_{1,4} = d_{1,5} = 1.48$, $d_{2,6} = d_{3,7} = d_{4,8} = d_{5,9} = 0.82$, and $d_{6,12} = d_{6,13} = d_{7,16} = d_{7,17} = d_{8,20} = d_{8,21} = d_{9,24} = d_{9,25} = 1.52$, $d_{6,10} = d_{6,11} = d_{7,14} = d_{7,15} = d_{8,18} = d_{8,19} = d_{9,22} = d_{9,23} = 1.64$. Radius of the round corners = 1.6.

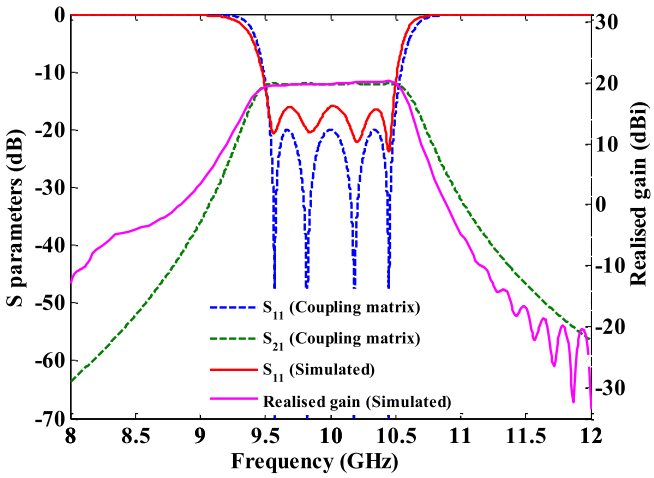

Fig. 10. Simulated frequency responses compared with the calculated of the fourth-order 4×4 *filtering planar antenna array*.

and control the spacing between the radiating outputs in the xz plane (E-plane). The dimensions obtained for the structure to generate the simulated results are given in the caption of Fig. 9.

V. Fabrication and Measurements

The seventh-order 4×4 *filtering planar antenna array* is fabricated from aluminum alloy 6082 using a Computer Numerical Control (CNC) milling machine, and is shown in Fig. 11. The CNC milling machine used here has a tolerance which is around ± 5 μm. To facilitate the fabrication process, the array is made out of three pieces, splitting along the E-plane of the waveguide cavities. This minimizes the effect of the additional loss occurring due to the imperfect joints in the pieces. Metal screws are used to assemble the pieces, and are

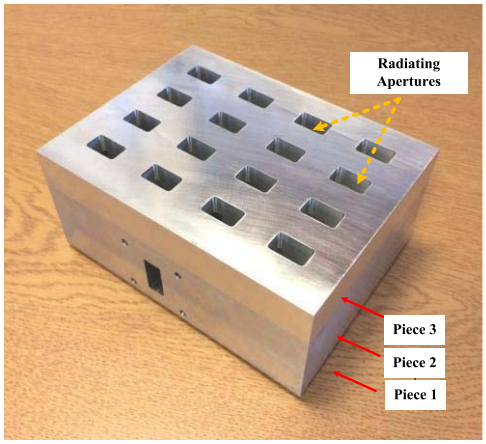

Fig. 11. Photograph of the fabricated seventh-order 4 × 4 filtering planar *antenna array*.

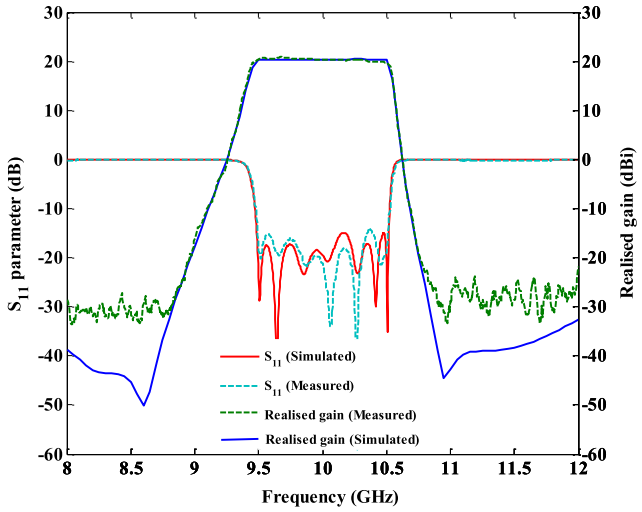

Fig. 12. Measured frequency responses compared with the simulated of the seventh-order 4 × 4 *filtering planar antenna array*.

inserted from the bottom in order to reduce the effect of the screw heads on the radiation performance.

In Figs. 12 and 13, the measured frequency responses are given and are compared with the simulated. It can be seen in Fig. 12 that the FBW, both in simulation and measurement, is more than 10% when $S_{11} = -15$ dB. The realized gain only fluctuates between 20.24 and 20. 43 dBi over the entire passband, and the 3-dB gain bandwith is 11%. The strong out of band rejections can be observed.

The radiation pattern for both the E- and H-planes are measured, and they are compared with the simulation in Fig. 13. The measured patterns are in good agreement with the simulation. The sidelobe level is lower than −12 dB at all frequencies within the passband in the E-plane and no beam squint is detected from antenna radiations patterns taken at the band edges (9.5 and 10.5 GHz.) However, in the *yz* plane (H-plane), because the spacing between the radiating apertures is large ($1.14\lambda_0$), two grating lobes can clearly be identified. Reducing the spacing between the radiating outputs in the H-plane for the given component is not possible due to

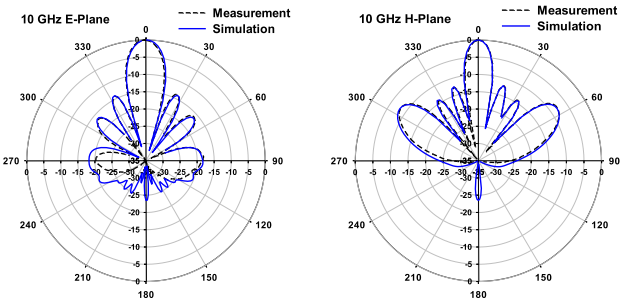

Fig. 13. Measured radiation pattern of the seventh-order 4 × 4 *filtering planar antenna array* compared with the simulated at center frequency 10 GHz for both the E- and H-planes.

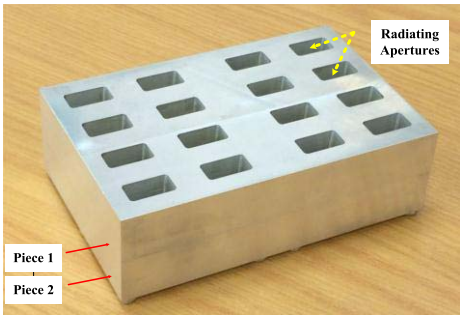

Fig. 14. Photograph of the fabricated fourth-order 4 × 4 *filtering planar antenna array*.

the electrically large dimensions of the waveguide resonators. However, it is possible to suppress the sidelobe levels when constructing the array based on the concept of unequal filtering power splitter [16] and will be the subject of future work.

Fig. 14 shows the photograph of the fabricated fourth-order 4 × 4 *filtering planar antenna array*. It is made out of two pieces of the aluminum alloy. The measured return loss and realized gain are shown in Fig. 15. They are in very good agreement with their simulations. The FBW is around 10% when S_{11} is −15 dB. Again, the realized gain is extremely flat over the frequency band of interest (9.5–10.5 GHz), having only 0.9 dB fluctuation. The peak gain is 20.32 dBi at frequency 10.45 GHz. The 3-dB gain bandwidth is 12%. There is a very good attenuation of the realized gain observed at the stopband, whilst it is slightly poorer at the start band. This is due to the nature of capacitive irises [32], [33]. The fourth-order 4 × 4 *filtering planar antenna array* maybe preferable over the seventh-order 4 × 4 *filtering planar antenna array* because of the lower number of layers and its reduced size.

The E- and H-planes radiation patterns of the 4 × 4 *filtering planar antenna array* are measured, and they are compared with the simulated ones in Fig. 16. It can be clearly seen that the sidelobe levels are below −13 dB in the E-plane. However, because of the large and inconsistent spacing, the sidelobe levels increase to −7.5 dB in the H-plane. Again no beam squint is detected for radiation patterns within the passband.

As commented previously, in the designs the resonators have to be accommodated within the structures whilst maintaining the same phase across the apertures. This has been achieved when the spacing between the radiating outputs

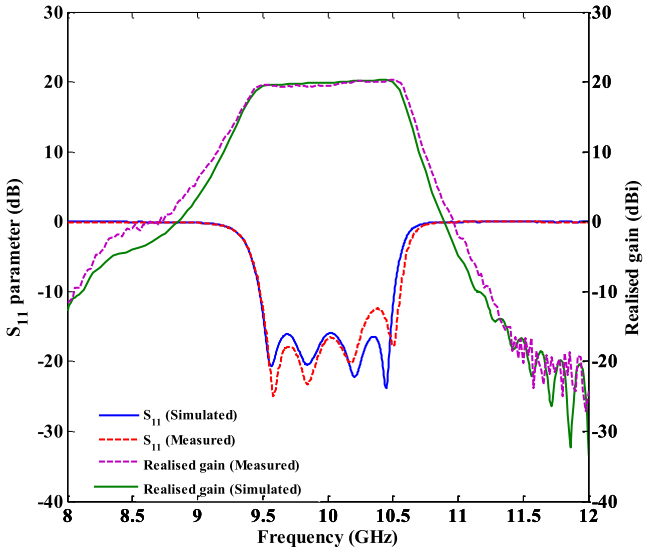

Fig. 15. Measured frequency responses compared with the simulated of the fourth-order 4×4 *filtering planar antenna array*.

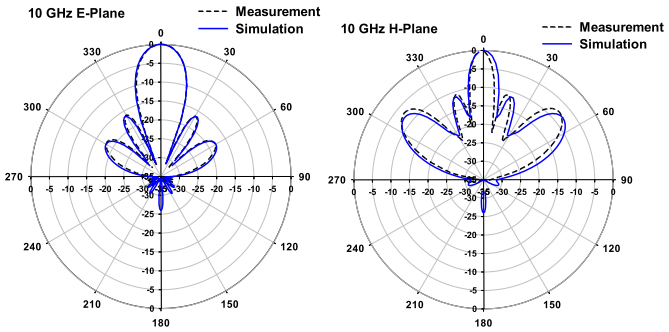

Fig. 16. Measured radiation pattern of the fourth-order 4×4 *filtering planar antenna array* compared with the simulated at center frequency 10 GHz for both the E- and H-planes.

is compromised to larger than 0.5 wavelengths, and also increasing non-radiating areas, particularly in the H-plane. This compromise has yielded a higher sidelobe levels in the H-plane, and lowered the aperture efficiency of just below 70% for both of the designs. Although higher aperture efficiency can be achieved in principle with larger than 0.5 wavelengths spacing this result is a compromise between efficiency and final size of the antenna whist accommodating the positing of the resonators. It should be mentioned that there are two other forms of losses which can contribute in the reduction of the efficiency of the designs as addressed in the following. The deigns are constructed from pieces (three pieces for Topology-I and two pieces for Topology-II). Although they are split along the E-plane of the waveguides (zero current line), there could be still some leakage of electromagnetic waves due to imperfect contact at the joints of the split pieces. On the other hand, the designs are built from Aluminum (Conductivity $= 3.56 \times 107$ S/m). Such Aluminum degrades the gain of the designs of about 0.5 dBi at the center frequency 10 GHz as obtained from CST simulation.

VI. Conclusion

A new synthesis approach for the design of high-gain and wide-bandwidth planar array antennas based on all resonator structures was presented in this paper. The approach was applied to two novel topologies. Topology I involved 39 resonators to build the 4×4 *filtering planar array* utilizing two waveguide-layers. Each resonator in topology I was connected to no more than three resonators. Topology II was also introduced in order to realize the 4×4 *filtering planar array* using only a single waveguide-layer and 25 coupled-resonators. Each resonator of topology II was connected to more than four resonators. Both of the topologies have been incorporated into physical structures using rectangular waveguide cavity resonators operating at *X*-band frequencies, and fabricated using the CNC milling machine. The measurements undertaken for the arrays were in a very good agreement with the simulations.

Acknowledgment

The authors would like to thank W. Hay at the School of Physics, University of Birmingham, Edgbaston, Birmingham, U.K., for fabricating the waveguide components.

References

[1] H. Guan-Long, Z. Shi-Gang, C. Tan-Huat, and Y. Tat-Soon, "Broadband and high gain waveguide-fed slot antenna array in the Ku-band," *IET Microwaves, Antennas Propag.*, vol. 8, no. 13, pp. 1041–1046, Oct. 2014.

[2] N. Goto, "A planar waveguide slot antenna of single layer structure," in *Proc. IEICE* Rep., 1988, pp. 88–39.

[3] K. Nidaira, T. Shirouzu, M. Baba, and K. Inoue, "Wireless IP access system for broadband access services," in *Proc. Eur. Conf. Wireless Technol.*, 2003, pp. 3434–3438.

[4] M. Ando, J. Hirokawa, T. Yamamoto, A. Akiyama, Y. Kimura, and N. Goto, "Novel single-layer waveguides for high-efficiency millimeter-wave arrays," *IEEE Trans. Microw. Theory Techn.*, vol. 46, no. 6, pp. 792–799, Jun. 1998.

[5] Y. Kimura *et al.*, "A low-cost and very compact wireless terminal integrated on the back of a waveguide planar array for 26 GHz band fixed wireless access (FWA) systems," *IEEE Trans. Antennas Propag.*, vol. 53, no. 8, pp. 2456–2463, Aug. 2005.

[6] J. Hirokawa, M. Zhang, and M. Ando, "94GHz single-layer slotted waveguide array by diffusion bonding of laminated thin plates," in *Proc. Int. Symp. Antenna Propag.*, 2008, pp. 907–911.

[7] J. Hirokawa, M. Ando, N. Goto, N. Takahashi, T. Ojima, and M. Uematsu, "A single-layer slotted leaky waveguide array antenna for mobile reception of direct broadcast from satellite," *IEEE Trans. Veh. Technol.*, vol. 44, no. 4, pp. 749–755, Nov. 1995.

[8] M. Ando, "Planar waveguide arrays for millimeter wave systems," *IEICE Trans. Commun.*, vol. 93, no. 10, pp. 2504–2513, 2010.

[9] M. Zhang, J. Hirokawa, and M. Ando, "An E-band partially corporate feed uniform slot array with laminated quasi double-layer waveguide and virtual PMC terminations," *IEEE Trans. Antennas Propag.*, vol. 59, no. 5, pp. 1521–1527, May 2011.

[10] J. Hirokawa, "Plate-laminated waveguide slot array antennas and its polarization conversion layers," *Autom.-J. Control, Meas., Electron., Comput. Commun.*, vol. 53, no. 1, pp. 9–19, Jan. 2017.

[11] S. Park, Y. Tsunemitsu, J. Hirokawa, and M. Ando, "Center feed single layer slotted waveguide array," *IEEE Trans. Antennas Propag.*, vol. 54, no. 5, pp. 1474–1480, May 2006.

[12] S. Fujii *et al.*, "A wideband single-layer slotted waveguide array with an embedded partially corporate feed," in *Proc. Int. Symp. Antennas Propag.*, Oct. 2008, p. TP-C27-5.

[13] S. S. Oh, J.-W. Lee, M.-S. Song, and Y.-S. Kim, "Two-layer slotted-waveguide antenna array with broad reflection/gain bandwidth at millimetre-wave frequencies," *IEE Proc.-Microw., Antennas Propag.*, vol. 151, no. 5, pp. 393–398, Oct. 2004.

[14] Y. Miura, J. Hirokawa, M. Ando, Y. Shibuya, and G. Yoshida, "Double-layer full-corporate-feed hollow-waveguide slot array antenna in the 60-GHz band," *IEEE Trans. Antennas Propag.*, vol. 59, no. 8, pp. 2844–2851, Aug. 2011.

[15] D. Kim, J. Hirokawa, M. Ando, J. Takeuchi, and A. Hirata, "4 × 4-element corporate-feed waveguide slot array antenna with cavities for the 120 GHz-band," *IEEE Trans. Antennas Propag.*, vol. 61, no. 12, pp. 5968–5975, Dec. 2013.

[16] G. L. Huang, S. G. Zhou, T. H. Chio, H. T. Hui, and T. S. Yeo, "A low profile and low sidelobe wideband slot antenna array FEB by an amplitude-tapering waveguide feed-network," *IEEE Trans. Antennas Propag.*, vol. 63, no. 1, pp. 419–423, Jan. 2015.

[17] A. E. Williams, "A four-cavity elliptic waveguide filter," in *Proc. G-MTT Int. Microw. Symp.*, 1970, pp. 90–93.

[18] A. E. Atia and A. E. Williams, "Narrow-bandpass waveguide filters," *IEEE Trans. Microw. Theory Tech.*, vol. 20, no. 4, pp. 258–265, Apr. 1972.

[19] J. S. Hong and M. J. Lancaster, *Microstrip Filters for RF/Microwave Applications*, 1st ed. New York, NY, USA: Wiley, 2001.

[20] M. J. Lancaster, "Radio frequency filter," W.I.P.O Patent WO/01/69712, Dec. 2001.

[21] T. F. Skaik, M. J. Lancaster, and F. Huang, "Synthesis of multiple output coupled resonator circuits using coupling matrix optimisation," *IET Microw. Antennas Propag.*, vol. 5, no. 9, pp. 1081–1088, Sep. 2011.

[22] X. Shang, Y. Wang, G. L. Nicholson, and M. J. Lancaster, "Design of multiple-passband filters using coupling matrix optimisation," *IET Microw., Antennas Propag.*, vol. 6, pp. 24–30, Jan. 2012.

[23] X. Shang, Y. Wang, W. Xia, and M. J. Lancaster, "Novel multiplexer topologies based on all-resonator structures," *IEEE Trans. Microw. Theory Techn.*, vol. 61, no. 11, pp. 3838–3845, Nov. 2013.

[24] Y. Yang and M. Lancaster, "Waveguide slot antenna with integrated filters," presented at the ESA Workshop Antennas Space Appl., Noordwijk, The Netherlands, Oct. 2010, pp. 48–54.

[25] H. T. Cheng, Y. Yusuf, and X. Gong, "Vertically integrated three-pole filter/antennas for array applications," *IEEE Antennas Wireless Propag. Lett.*, vol. 10, pp. 278–281, 2011.

[26] H. Chu, J.-X. Chen, S. Luo, and Y.-X. Guo, "A millimeter-wave filtering monopulse antenna array based on substrate integrated waveguide technology," *IEEE Trans. Antennas Propag.*, vol. 64, no. 1, pp. 316–321, Jan. 2016.

[27] C. K. Lin and S. J. Chung, "A filtering microstrip antenna array," *IEEE Trans. Microw. Theory Techn.*, vol. 59, no. 11, pp. 2856–2863, Nov. 2011.

[28] X. Xu, J. Hirokawa, and M. Ando, "A waveguide slot array antenna with integrated T-shaped filters in the corporate-feed circuit," in *Proc. Int. Symp. Antennas Propag. (ISAP)*, Nov. 2015, pp. 1–2.

[29] *C. M. Studio*, Computer Simulation Technology AG, Darmstadt, Germany, 2009.

[30] J. S. Hong and H. Shaman, "An optimum ultra-wideband microstrip filter," *Microw. Opt. Technol. Lett.*, vol. 47, no. 3, pp. 230–233, Nov. 2005.

[31] J. S. Hong and M. J. Lancaster, "Cross-coupled microstrip hairpin-resonator filters," *IEEE Trans. Microw. Theory Techn.*, vol. 46, no. 1, pp. 112–118, Jan. 1998.

[32] J. A. R. Cruz, K. A. Zaki, J. R. M. Garai, and J. M. Rebollar, "Rectangular waveguide elliptic filters with capacitive and inductive irises and integrated coaxial excitation," in *IEEE MTT-S Int. Microw. Symp. Dig.*, Jun. 2005, pp. 269–272.

[33] X. Shang, M. Ke, Y. Wang, and M. J. Lancaster, "Micromachined W-band waveguide and filter with two embedded H-plane bends," *IET Microwav., Antennas Propag.*, vol. 5, no. 3, pp. 334–339, Feb. 2011.

[34] M. J. Lancaster, *Passive Microwave Device Applications of Superconductors*. Cambridge, U.K.: Cambridge Univ. Press, 1997, ch. 4, pp. 126–143.

[35] J. Aitken, "Swept-frequency microwave Q-factor measurements," *Proc. IEE*, vol. 123, no. 9, pp. 855–862, Sep. 1976.

[36] C. Carceller, P. Soto, V. Boria, M. Guglielmi, and J. Gil, "Design of compact wideband manifold-coupled multiplexers," *IEEE Trans. Microw. Theory Techn.*, vol. 63, no. 10, pp. 3398–3407, Oct. 2015.

[37] P. Soto, V. E. Boria, C. Carceller, S. Cogollos, M. Guglielmi, and D. Smacchia, "Practical design of rectangular waveguide filters with a capacitive building block providing an extra transmission zero," in *IEEE MTT-S Int. Microw. Symp. Dig.*, May 2015, pp. 1–4.

Rashad H. Mahmud was born in Erbil-Kurdistan Region, Iraq, in 1986. He received the B.Sc. (Hons.) degree in physics and the M.Sc. (Hons.) degree in electromagnetics from Salahaddin University-Erbil, Erbil, Iraq, in 2007 and 2010, respectively, and the Ph.D. degree in microwave engineering from the University of Birmingham, Birmingham, U.K., in 2016, with a focus on micromachined terahertz waveguide circuits such as antennas and filters.

He is currently with the Physics Department, Salahaddin University-Erbil, Kurdistan Region, Iraq. His current research interests include the synthesis and integrate of microwave multiport distribution networks/circuits with inherent filter transfer functions based on all-resonator circuits.

Michael J. Lancaster (SM'04) was born in England, in 1958. He received the B.Sc. degree in physics from the University of Bath, Bath, U.K., in 1980, and the Ph.D. degree in 1984, with a focus on nonlinear underwater acoustics.

He was a Research Fellow with the Surface Acoustic Wave (SAW) Group, Department of Engineering Science, Oxford University, Oxford, U.K., where he was involved in the design of new, novel SAW devices, including RF filters and filter banks. In 1987, he joined the Department of Electronic and Electrical Engineering, University of Birmingham, Birmingham, U.K., as a Lecturer of Electromagnetic Theory and Microwave Engineering, where he focused on the study of the science and applications of high-temperature superconductors and microwave frequencies. He joined the Head of the Department of Electronic, Electrical and Systems Engineering, University of Birmingham, in 2003. He is currently a Chartered Engineer and Chartered Physicist, University of Birmingham. He has authored two books and over 190 papers in refereed journals. His current research interests include microwave filters and antennas, high-frequency properties and applications of a number of novel and diverse materials, and micromachining as applied to terahertz communications systems

Dr. Lancaster is a Fellow of the IET and the U.K. Institute of Physics. He has served on the MTT IMS Technical Committee.